ウェブサイト公開用

(様式 10)
(海外特別研究員事業)
令和１年１２月３１日

海 外 特 別 研 究 員 最 終 報 告 書

独立行政法人日本学術振興会 理事長　殿

採 用 年 度　平成 30 年度
受 付 番 号　201860028
氏　　　名　石井 琢郎
(氏名は必ず自署すること)

海外特別研究員としての派遣期間を終了しましたので、下記のとおり報告いたします。
なお、下記及び別紙記載の内容については相違ありません。

記

1. 用務地（派遣先国名）用務地：　ウォータールー大学　　　（国名：　カナダ　　　）

2. 研究課題名（和文）※研究課題名は申請時のものと違わないように記載すること。
高速超音波撮像法を用いた排尿流可視化による排尿機能評価ツールの開発

3. 派遣期間：平成　３０　年　４　月　１　日　～　令和　１　年　１２　月　６　日

4. 受入機関名及び部局名
University of Waterloo, Department of Electrical and Computer Engineering

5. 所期の目的の遂行状況及び成果…書式任意　**書式任意（A4 判相当 3 ページ以上、英語で記入も可）**
（研究・調査実施状況及びその成果の発表・関係学会への参加状況等）
（注）「6. 研究発表」以降については様式 10－別紙 1～4 に記入の上、併せて提出すること。

1. Summary

Working on the proposed research directions, I have devoted myself into establishing a high-frame rate ultrasound system for urodynamic imaging. Achievements in the research project are summarized in three pillars: 1) a novel contrast-enhanced high-frame rate ultrasound framework (CE-UroVPI) that is specifically designed for imaging physiological urinary flow dynamics; 2) a new testbed design and its fabrication protocol that resembles geometric, mechanical and hydrodynamic properties of a male urinary tract during voiding; and 3) performance evaluation tests of CE-UroVPI framework by visualization of the simulated urinary flow in the new testbed system.

The performance evaluation showed CE-UroVPI framework successfully visualized a time-resolved urinary flow dynamics with characteristic complex flow patterns in a diseased urinary tract with patho-anatomical features of benign prostatic hyperplasia. In addition, the observed flow dynamics was quantified using spatio-temporal distribution of the flow speed and direction measured by CE-UroVPI, and the characteristic flow dynamic events in the diseased model were identified quantitatively. These results asserts the devised imaging method is capable of visualizing precise spatio-temporal urinary flow dynamics that would facilitate hydrodynamic assessments as a novel diagnostic method for urinary voiding disorder.

During the period of the JSPS fellowship, I have submitted two original papers and one of those papers has been published in Medical Physics, a top-tier journal in my research filed. Also, I have co-authored two papers that report on novel robust, real-time vector flow imaging methods. Furthermore, I have made two presentations and contributed to four presentations at IEEE International Ultrasonics Symposiums in 2018 and 2019.

In conclusion, throughout the research project, a novel ultrasound imaging framework for visualizing complex urinary flow dynamics was developed, and fundamental performance and preliminary clinical feasibility of the framework were investigated using anthropomorphic phantoms. These achievements facilitate further development of a new diagnostic tool for the urinary voiding dysfunction using a new ultrasound urodynamic imaging system that will be carried out in my future project.

2. Development of CE-UroVPI framework

Framework Design and Implementation

I have formulated a new high frame rate ultrasound (HiFRUS) imaging framework called contrast-enhanced urodynamic vector projectile imaging (CE-UroVPI) that can spatiotemporally resolve the dynamics of urinary tract and associated complex flow patterns (Figure. 1).

This framework was implemented on a workstation that was connected to a programmable ultrasound scanner in order to process the received RF signal on-line.

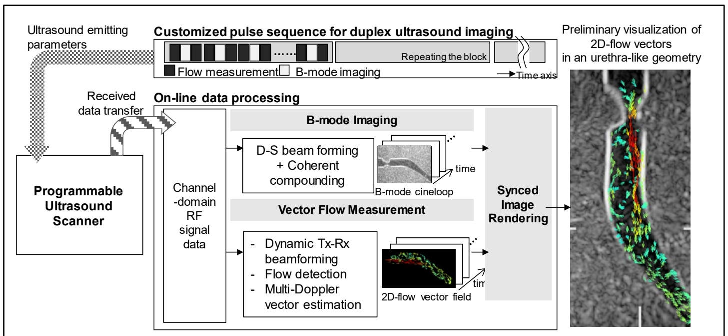

Figure 1. Outline of the CE-UroVPI framework

This new framework has three important technical features:

1) CE-UroVPI can achieve high frame rates of 1,250 frames per a second (fps) that are well beyond the video display rate achievable in conventional ultrasound imaging; the corresponding sub-millisecond time resolution, coupled with full-view imaging capability, is suitable to resolve spatiotemporal dynamics that occur in a urinary tract deformation episode;
2) CE-UroVPI uses microbubbles as contrast agents to overcome inherent concerns with weak urine signal strength; and
3) CE-UroVPI has leveraged recent innovations in HiFRUS to map flow vector patterns (i.e. both flow speed and flow direction) and rendering them through a dynamic visualization algorithm called vector projectile imaging (VPI).

In particular, the flow vector patterns mapping process employs a robust Doppler-vector estimation algorithm called extended-least square vector Doppler (ELSVD) method. In this method, aliasing artefacts presenting in raw Doppler maps in urinary flow imaging (Fig. 2 Top) can be corrected adaptively by applying block-matching method to contrast-enhanced flow speckle images. As a result, consistent flow patterns were successfully visualized as shown in Fig. 2 (Bottom).

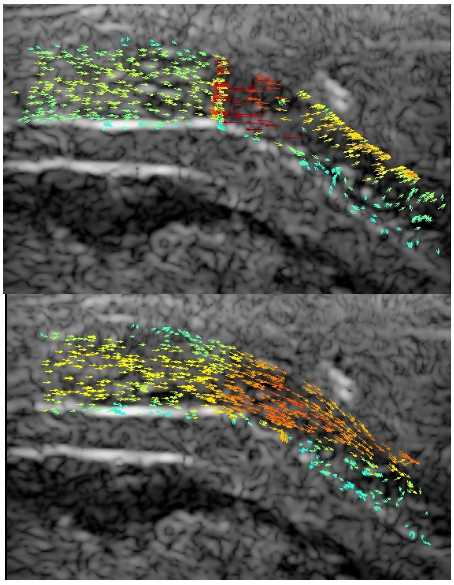

Figure 2. Adaptive correction of aliasing artefacts. Vector flow visualization without ELSVD (Top) and with ELSVD (Bottom)

A GPU implementation of Robust Vector Flow Imaging Framework

Despite of the robust performance of vector flow estimation in CE-UroVPI method, ELSVD algorithm's high-computational complexity makes it challenging to adopt for real-time use. In cooperation with the present research group, we have implemented the ELSVD method leveraging the parallel computing capability of GPGPU and CUDA library in order to achieve the real-time capability of CE-UroVPI framework. The framework was built on three levels of parallelization:

1) Frame level (ELS-VD applied on every pixel);
2) Pixel level (multiple least square systems per pixel);
3) Operation level (parallelized matrix computations).

ELS-VD was structured as six cascades of resource optimized GPU kernels, and it was implemented using CUDA and a GTX 1080 device.

As shown in Fig. 3, 160K and 62.5K pixels of robust flow vectors were computed in less than 40 ms (video range) for maximum aliasing order 1 and 2 respectively. These numbers are well beyond number of flow-region pixels in the urinary flow images (< 50 kPixels).

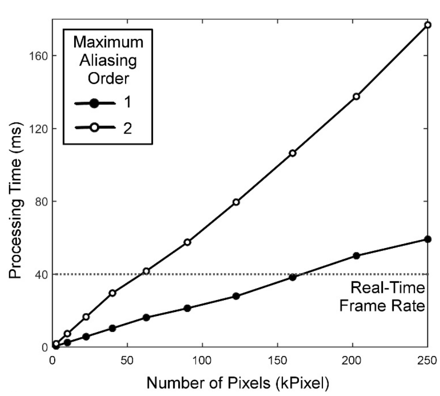

Figure 3. Benchmark of GPU-ELSVD framework

3. Design and Fabrication of Deformable Urinary Tract Phantom

To carry out performance evaluation and fine tuning of the CE-UroVPI framework, I have devised deformable urinary tract phantoms with and without urethral obstructions; these phantoms were designed to resemble geometric, mechanical and hydrodynamic properties of the urinary tract. Specifically, they possess two important functional characteristics: first, to mimic pre-voiding status, the urinary tract would remain collapsed when there was no internal flow; and second, to mimic a voiding episode, the flow tract would expand and form a realistic urinary tract in response to an increase in hydraulic pressure at the inlet.

All urethra phantoms fabricated using a new protocol were consisted of three major components (Fig.4): (i) a thin-walled flexible urinary tract tube (PVA urethra) that was designed based on anatomically realistic geometries and dimensions; (ii) a tissue slab that resembled the elastic properties of prostatic tissues surrounding the urethra; (iii) a calibrated flow circuit that was responsible for instigating and maintaining the course of a voiding episode.

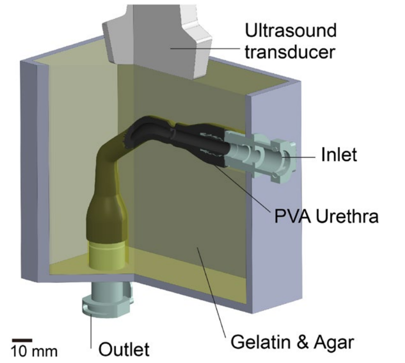

Figure 4. Outline of a Deformable Urinary Tract Phantom

Thin-Walled Flexible Urinary Tract Tube

First, an inner geometry of urinary tract was drafted to resemble a normal male urethra's intra-luminal shape at maximum voiding flow rate (i.e. when the urethra was in its most expanded form). This urinary tract geometry (Fig. 5) was based on published data on anatomic dimensions of the urinary tract (such as length and angle) and the urethral opening (such as shape and diameter). In addition, to construct a diseased urethra phantom with benign prostatic hyperplasia (BPH) feature, the inner core of the normal urinary tract was modified by adding a feature of lateral-lobe protrusion to the geometry (Fig.5 Middle).

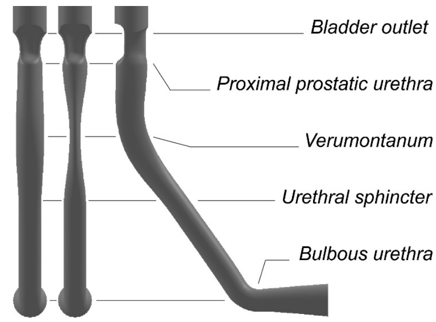

Figure 5. Inner geometry of the urinary tract. Coronal projection view of the normal model (Left), and the BPH model (Middle), and sagittal projection view of both models (Right). Labels indicate transversal planes used to define the geometries.

Next, an outer-mold of the tube phantoms was designed as shown in Fig. 6. The outer-wall geometry was defined by radially expanding the dimensions of the normal urinary tract geometry along the entire tract by 3mm. In doing so, a 3mm radial gap would exist between the inner core and the outer mold's cavity wall. In contrast, with the inner core for the BPH-featured diseased urethra, the radial gap would range from 3mm at certain parts of the tract to 4.5 mm at the Verumontanum whose short-axis diameter was reduced by 40% relative to the normal urethra. All inner and outer-design of the tube phantoms were drafted using Solidworks and printed using a 3-D printer.

Finally, a mixture solution of 8% poly-vinyl alcohol (PVA) and 1% graphite as acoustic scatterers was injected to fill the cavity between the inner core and the outer-wall of the mold. Subsequently, the mixture-filled mold was put through two cycles of freeze-thaw process (24 hours of -20°C freezing followed by 24 hours of 5°C thawing). In doing so, a PVA-thin-walled flexible urinary tract tube was achieved (Fig. 6 e). It was found that the PVA tube had a Young's elastic modulus of 26.6±4.0 kPa that falls within the expected range of the urethra's elasticity.

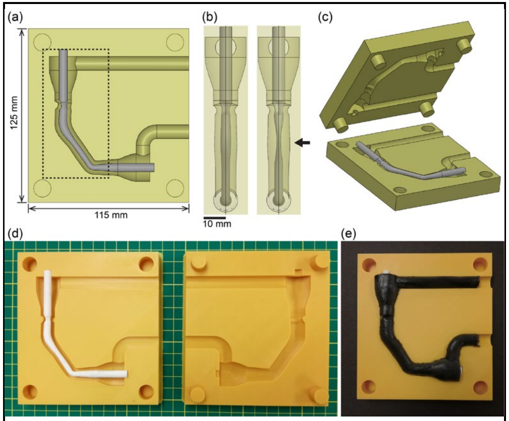

Figure 6. Top row: the outer-mold design; Bottom row: a set of 3-D printed core and outer-molds, and a casted PVA tube.

Tissue Slab to Mimic Urethral Mechanical Properties

With the fabricated urinary tract, an anatomical phantom of the urethra was formed by casting a prostatic tissue-mimicking layer around the PVA tract (Fig. 7). First, the PVA-urinary tract was placed onto an imaging box using two flow connectors, and the box's open volume was filled with degassed water. Next, a 20cc syringe was connected to the inlet of the urinary tract to suck air out of the tract lumen; in doing so, the urinary tract was collapsed so as to mimic shape of a pre-voiding urinary tract. Finally, an agar-gelatin mixture consisted of 93.7% water, 1.0% agar and 5.0% gelatin and 0.3% potassium sorbate preservatives was filled in the open volume of the imaging box. The filled phantom box was subsequently placed in a refrigerator for 6 hours to allow the agar-gelatin mixture to solidify and form a slab. The Young's modulus of the tissue slab was found to be 17.4±3.4 kPa, which is within the range of elasticity values for human prostate.

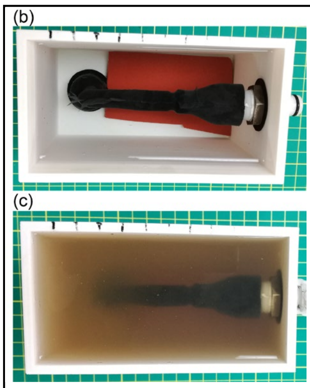

Figure 7. A urinary tract phantom before (Top) and after (Bottom) casting a tissue slab

Flow Circuit for Simulation of Voiding

The inlet and outlet of the urinary tract phantom were connected to a flow circuit to simulate urinary passage and urethral wall deformation during voiding. The phantom inlet was connected to a custom-designed gear pump that was programmed to deliver a single flow pulse in each experiment run. The "on" state of the flow pulse was set to deliver constant flow at a rate of 7 mL/s for 1 second, which is clinically regarded as the threshold flow rate for patients with severe voiding dysfunction. Such flow pattern assumed constant bladder contraction.

Ultrasound Imaging Experiments

To demonstrate the functional characteristics of the developed urinary tract phantoms, ultrasound imaging experiments were performed.

First, the urethra phantoms fabricated using our new protocol were found to be effective in resembling urethral wall deformation during voiding. Three B-mode images for the mid-sagittal view of the normal urethra phantom in the initial state (at 0s), during voiding (at 1 s), and at the end of a voiding episode (at 2 s). As can be observed, the PVA-based urinary tract was collapsed before the start of voiding and was embedded within the tissue mimicking slab (Fig. 8 Left-a). When the flow pump was turned on, the increase in fluid pressure within the urinary tract led to the formation of a flow channel. Accordingly, the urinary tract was expanded, resulting in the creation of a hypoechoic lumen region in the B-mode image (Fig. 8 Left-b). After the flow pulse had ended and the remaining fluid within the urinary tract was discharged, the PVA tube returned to its original collapsed form (Fig. 8 Left-c). This deformation sequence can be stably produced over multiple simulated voiding cycles.

Next, Doppler images for both normal and diseased (BPH) models showed hydrodynamic characteristics of each urethra phantom. The key observation to be noted is that, in the BPH model, a flow jet was formed downstream from the urethral obstruction as marked by the arrows in Fig. 8 Right-b. Such feature was not observed in the normal urethra phantom (Fig. 8 Right-a). In the jet region of the BPH phantom, the spatial-maximum axial flow speed (without Doppler angle correction) was measured to be 59.3±5.8 cm/s (temporal mean over 5 color Doppler image frames). This value is significantly higher ($p<0.001$, paired t-test) than the spatial-maximum axial flow speed of 22.7±9.0 cm/s measured in the normal urethra phantom.

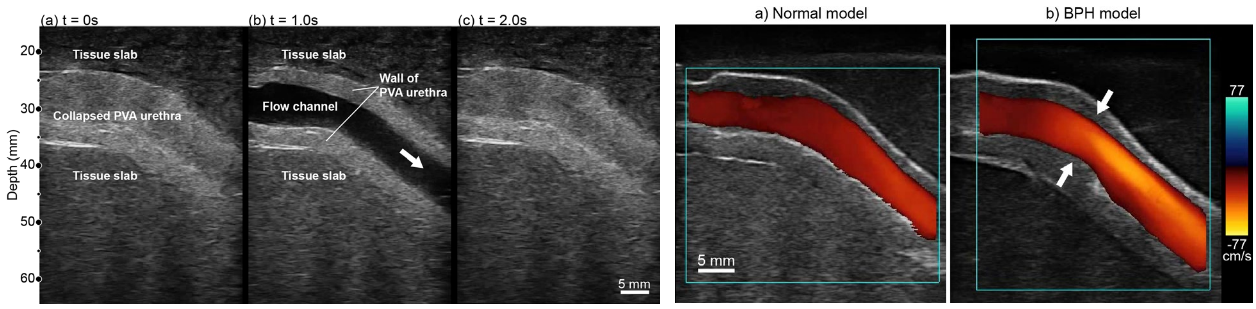

Figure 8. Left: B-mode images of the normal urinary tract phantom in initial state (a), during voiding (b), and at the end of a voiding episode. Right: Doppler color map of internal flow profile during voiding in both normal (a) and BPH (b) models.

4. Vector Projectile Imaging of Dynamic Urinary Flow in the Deformable Urinary Tract Phantoms

To confirm the efficacy of the CE-UroVPI framework, I have carried out an experiment to image urinary flow in the developed urinary tract phantoms. Fig. 9 shows urinary flow vectors in normal and BPH models at maintenance phase (t = 1.0 s). As can be observed, flow profiles in the diseased (BPH) model show characteristic flow patterns such as a flow jet and flow recirculation; these complex flow patterns were not observed in conventional Doppler images (Fig. 8 right).

In addition, Fig. 10 shows time-resolved visualization of the urinary flow dynamics during initiating phase of voiding. The high-frame rate imaging capability of CE-UroVPI framework successfully visualizes precise fluid-structural interaction of the urinary flow both in normal and BPH models.

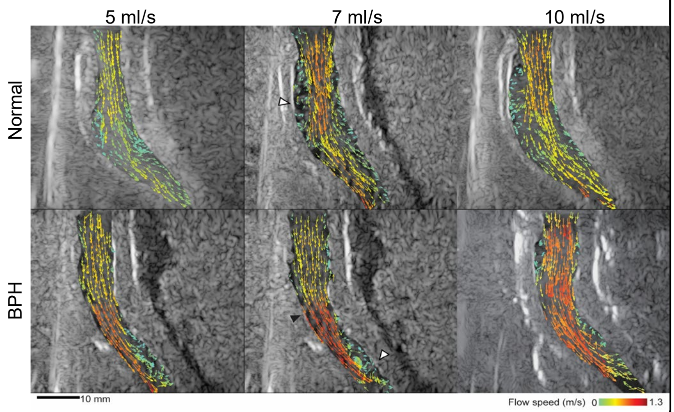

Figure 9. Vector projectile imaging of normal (Top row) and diseased (Bottom row) models at different flow rates.

These results assert the new imaging framework will provide new insights into hydromechanical causal mechanisms of voiding symptoms. In the second-year projects, I will develop hydrodynamic characterization algorithms that quantitatively visualize these spatial-temporal urodynamic properties.

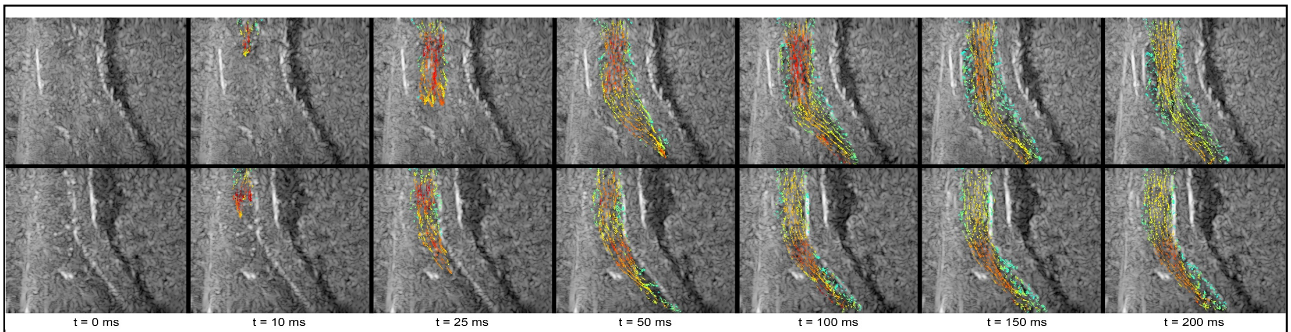

Figure 10. Time-resolved visualization of urinary flow in normal (Top row) and diseased (Bottom row) models with a 7ml/s maximum flow rate setting at different points in time.

Quantitative Characterization of the Urinary Flow Dynamics Observed in the Urinary Tract Phantoms

The visualized urinary flow dynamics was further quantitatively assessed using both temporal and spatial variability of flow speed and direction. Figure 11 shows a series of time plots that depict the median and interquartile range (IQR) of cross-sectional flow speeds at different axial differences (5, 10, 20, 30 mm) away from the bladder outlet. It can be observed that, in the BPH-obstructed urethra, there was a transient surge in flow speed in the first 100 ms (blue line in Fig. 11). Following this transient surge, flow velocities were found to vary spatially at different axial positions during the maintenance phase of voiding. At 5 mm away from the bladder outlet, the spatial-median speed peaked at 1.20 m/s, and it was reduced to 0.58 m/s after the first 100 ms. In contrast, the extent of temporal variability was smaller at 20 mm axial distance where the verumontanum narrowing was located. Here, the spatial-median speed reached a maximum of 0.91 m/s within the first 100 ms, and afterward it was slightly reduced to 0.76 m/s. These spatiotemporal trends were found to be different from

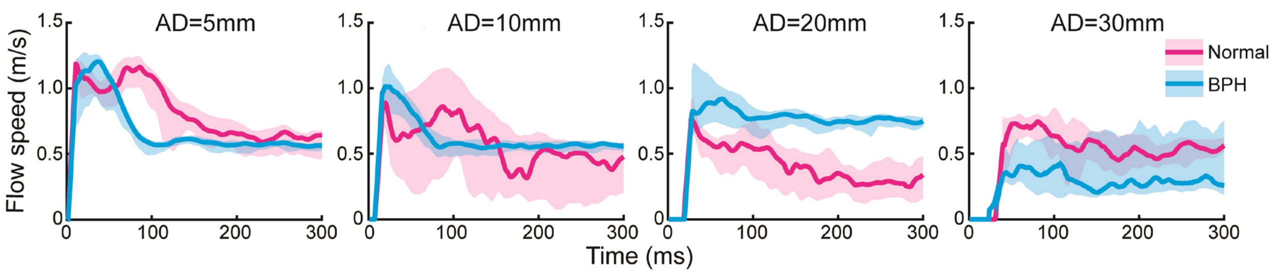

Figure 11. Temporal variability of flow speed on different axial distances away from the bladder outlet, with ieach line and colored zone respectively indicating spatial-median flow speed and the interquartile range of flow speeds at that axial distance (AD) away from the bladder outlet.

those observed for the normal urethra (red line in Fig. 11).

CE-UroVPI revealed further differences in the urodynamics of the two urethra geometries during the maintenance phase of voiding when the urinary tract was expanded. Fig. 12 shows spatial variabilities in flow speed and direction for the different axial distances (0-30 mm in 5 mm steps) from the bladder outlet in the normal and BPH-obstructed urethra phantoms at 300ms after the onset of voiding. The primary finding to be noted from these results is that, during the maintenance phase of voiding, the BPH-obstructed urethra had faster flow speeds at the site of verumontanum narrowing (20 mm away from the bladder outlet; indicated by solid triangle marker in Fig. 12). The spatial-median velocity at this axial location was 0.77 m/s, and it was higher than that for the normal urethra (0.28 m/s) at the same location (statistically different; $p < 0.001$). Flow was generally unidirectional (with only a 2.4° angle span) in the BPH-obstructed urethra at this axial location.

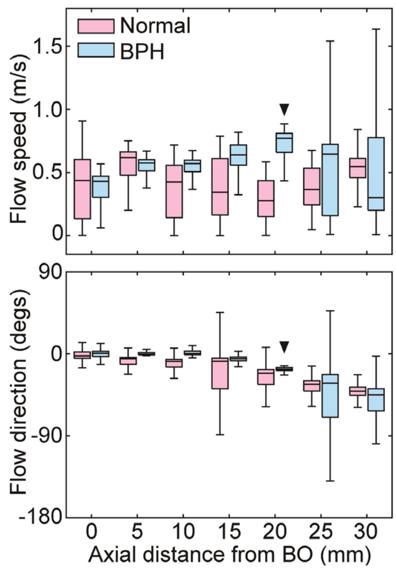

Figure 12. Flow speed and angle distribution of maintenance phase of voiding (t=300ms) observed by CE-UroVPI.

Another observation of interest in Fig. 4b is that the flow profile downstream from the verumontanum narrowing was separated into two spatial zones: a high-speed jet zone and a low-speed vortex region. This flow separation feature was not found in the normal urethra. Accordingly, at 30 mm away from the bladder outlet, the BPH-obstructed urethra exhibited a large range of flow speeds, whereby the spatial-maximum and spatial-median flow speeds were respectively 1.64 m/s and 0.30 m/s. Such flow speed distribution was found to have a statistically significant difference from that for the normal urethra at the same location ($p < 0.001$). The corresponding flow directions for the BPH-obstructed urethra spanned a larger range of angles (24.3°) as compared to the normal urethra (9.0°).

5. Publications and Conference Presentations

Throughout my JSPS overseas research project, I have written and submitted two original manuscripts in order to report the achievements from the project. One of those was about the new fabrication protocol of the deformable urinary tract phantom and it has been published in Medical Physics, a well-recognized journal in biomedical engineering. In addition, I have submitted another manuscript about a novel ultrasound urodynamic imaging framework, CE-UroVPI, and its fundamental performance for publication in Urology, which is a top-tier journal in urology. This manuscript is now under consideration for publication.

Also, I have made two presentations regarding a novel ultrasound urodynamic imaging framework and also contributed to four other presentations, which were co-authored by my colleagues at University of Waterloo, at a top-tier international ultrasound conference, IEEE International Ultrasonics Symposium held from October 22nd to 25th, 2018 in Kobe, Japan, and from October 7th to 9th, 2019 in Glasgow, UK.